Estimating Measurement Uncertainty on Stress-Strain Curves from SHPB

Denis Brizard, Sylvie Ronel, Eric Jacquelin

Noname manuscript No.
(will be inserted by the editor)

Estimating measurement uncertainty on stress-strain curves from SHPB

D. Brizard · S. Ronel · E. Jacquelin

the date of receipt and acceptance should be inserted later

Abstract Split Hopkinson Pressure Bar tests are commonly used to determine material stress-strain relationship at high deformation rates. Obtaining this relationship is dependant both on certain assumptions and substantial post-processing of the data recorded during the test. Measurement uncertainty rarely appears on the resulting curves. This article introduces a simple method of estimating the measurement uncertainty associated with SHPB tests.

Keywords Measurement uncertainties, Split Hopkinson Pressure Bars, Propagation of uncertainty

1 Introduction

Split Hopkinson Pressure Bars (SHPB) are commonly used today to characterize materials in the $100\,\mathrm{s}^{-1}$ to $10\,000\,\mathrm{s}^{-1}$ strain rate range [1]. The device and the corresponding treatment of measurements developed substantially during the second half of the twentieth century [2,3]. The first measuring bars were metallic, used for the characterization of high impedance materials [4]. Subsequently, the use of polymeric –low impedance– measuring bars and the development of the associated post-processing enabled lower impedance samples

D. Brizard
Univ Lyon, Université Claude Bernard Lyon 1, IFSTTAR, LBMC UMR_T9406, F69622, Lyon, France
E-mail: denis.brizard@ifsttar.fr

S. Ronel
Univ Lyon, Université Claude Bernard Lyon 1, IFSTTAR, LBMC UMR_T9406, F69622, Lyon, France
E-mail: sylvie.ronel@univ-lyon1.fr

E. Jacquelin
Univ Lyon, Université Claude Bernard Lyon 1, IFSTTAR, LBMC UMR_T9406, F69622, Lyon, France
E-mail: eric.jacquelin@univ-lyon1.fr

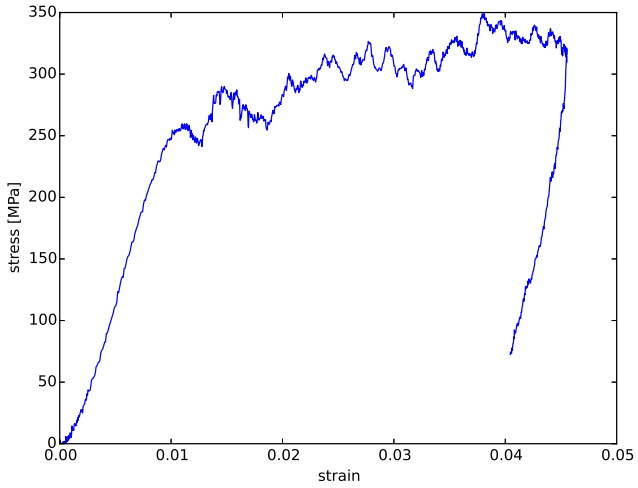

Fig. 1: Example of stress-strain curve obtained with an SHPB device: copper sample at $1300\,\mathrm{s}^{-1}$

such as polymeric foams to be tested [5]. The SHPB device –initially designed for compression testing– was then adapted to tension testing, torsion testing and shear testing. It was also modified to test ceramic materials or concrete [1]; it has recently been used in the field of biomechanics to test biological tissues [6,7,8].

Figure 1 illustrates a typical stress-strain curve obtained with an SHPB setup. As for any experimental data, the graph should display measurement uncertainty, for each experimental point. In addition, the derivation of the stress-strain relationship is based on the assumption of stress equilibrium in the sample, which requires a certain ring-up time. It would therefore be interesting to plot the point beyond which the sample is at equilibrium on the final stress-strain plot, especially if pulse shaping techniques [9,10] are not employed.

To the authors' knowledge, the time from which the sample is at equilibrium never appears on the SHPB stress-strain curve and the question of measurement uncertainty on resulting stress-strain curves has not yet been addressed clearly.

The first part of this article (Section 2) briefly recalls the operating principle of a Split Hopkinson Pressure Bar apparatus and the underlying equations for the stress and strain in the sample. Measurement uncertainty is analyzed according to its three sources in Sections 3 to 5. The first source of uncertainty is the strain-measuring device, which converts the strains in the bars into amplified electrical signals (strain gauges, excitation device, amplifier, digital sampling oscilloscope); these recorded voltages are then converted into strains (Section 3). The second source of uncertainty is the conversion of the

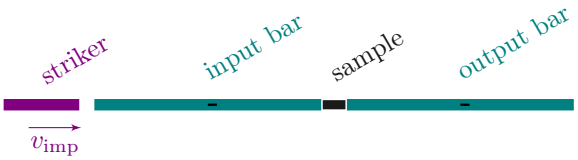

Fig. 2: Split Hopkinson pressure bar setup

strain in the measuring bars into stress and strain in the sample held between the bars (Section 4). The third source of uncertainty is the propagation of the strain signals from the actual strain gauge positions to the bar-sample interfaces (Section 5). In the last section, all these measurement uncertainties are combined, yielding the total uncertainty on the stress-strain curve (Section 6).

2 SHPB setup and input uncertainties

2.1 Operating principle

The classic SHPB setup consists of two long bars (Figure 2), between which the sample is placed. A compressive strain wave, generated by a striker, propagates through the input bar, the sample and then the second, or output, bar. Two conditions are required to avoid superposition of the incident and reflected waves in the input bar. First, the strain gauges, glued onto the surface of the bar, must be located half-way along the bar; second, the length of the striker must also be such that the length of the strain wave is shorter than half the length of the incident bar. The strain gauge on the input bar measures the incident $\epsilon_i(t)$ and reflected $\epsilon_r(t)$ strain waves, the strain gauge on the output bar measures the transmitted strain wave $\epsilon_t(t)$.

Figure 3 details the main steps to obtain the stress-strain relationship in the sample ($\sigma_s(t)$, the stress in the sample, as a function of $\epsilon_s(t)$, the strain in the sample) from the strains measured $\epsilon_i(t)$, $\epsilon_r(t)$ and $\epsilon_t(t)$ in the middle of the bars. Obtaining the stress-strain relationship of the sample is not straightforward: it requires the measurement of the strain in the two measuring bars and is dependent on certain assumptions (see [3] for a detailed discussion), which include the force equilibrium in the sample.

Once the sample reaches stress equilibrium, the strain rate, strain and stress in the sample are given by

$$\dot{\epsilon}_s(t) = \frac{-2c_0}{l_s}\epsilon_r(t) \tag{1}$$

$$\epsilon_s(t) = \frac{-2c_0}{l_s}\int_0^t \epsilon_r(\tau)d\tau \tag{2}$$

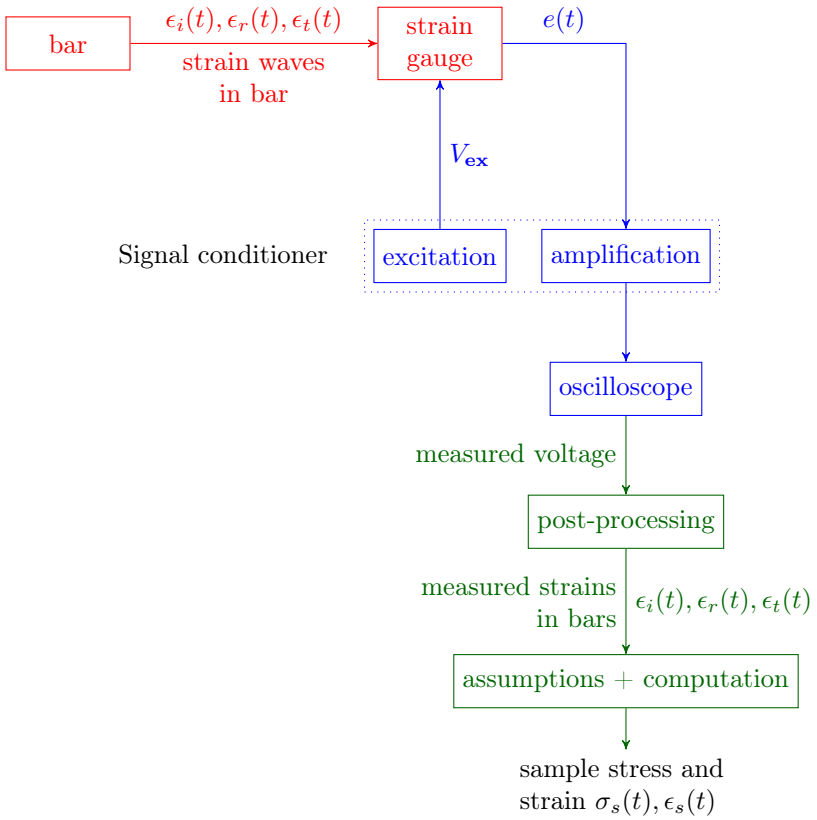

Fig. 3: Diagram of information flux for SHPB test processing (physical quantities, electrical quantities, post-processing/numerical data)

$$\sigma_s(t) = \frac{A_b E_b}{A_s} \epsilon_t(t) \tag{3}$$

where c_0 is the wave velocity of the measuring bars, l_s is the initial length of the sample, E_b is the Young modulus of the bars, A_b is the cross section of the output measuring bar, and A_s is the initial cross section of the sample.

2.2 Description of our device and associated input uncertainties

The following is a description of the specific SHPB device designed and built at our laboratory, LBMC UMR_T9406 (Ifsttar/UCBL).

The measuring bars are made of Armco 17-4PH precipitation-hardening steel with a Poisson's coefficient of $\nu = 0.291$ according to the manufacturer. The uncertainty on ν concerns its last significant digit ($0.29\underline{1}$) and following

[11] (Rule 1, page 23), the absolute uncertainty on ν is taken as $u(\nu) = 0.0005$. The bar velocity c_0 and Young modulus E_b are supposed to be experimentally determined to within 0.1 %.

$$\frac{u\left(c_0\right)}{c_0} = 0.1\,\% \tag{4}$$

$$\frac{u\left(E_b\right)}{E_b} = 0.1\,\% \tag{5}$$

We adopt here the common notations for measurement uncertainty where $u(a)$ denotes the standard uncertainty in a.

The bars are centerless ground to the nominal diameter of 31.75 mm. The diameter is measured at several points and ranges from 31.71 mm to 31.76 mm, so the absolute uncertainty on the diameter is 0.025 mm

$$u(d_b) = 0.025\,\text{mm} \tag{6}$$

The gauge signal conditioner is a Dewetron HSI-STG module [12], powered by a Dewetron DEWE-30-8 chassis. The range of the input voltage is 10 mV. The module's input voltage accuracy is stated as "$\pm$0.05 % of reading$\pm$ 0.02 % of range $\pm$ 10 µV" so

$$u(e_{\text{HSI}}(t)) = \pm 0.05\,\% \times e(t) \pm 0.02\,\% \text{ of range} \pm 10\,\mu\text{V} \tag{7}$$

where $u(e_{\text{HSI}}(t))$ is the uncertainty on the voltage $e(t)$ due to the signal conditioner. The excitation voltage V_{ex} is set to 5 V and the excitation voltage accuracy is

$$u(V_{\text{ex}}) = \pm 0.03\,\% \times V_{\text{ex}} \pm 1\,\text{mV} \tag{8}$$

The analog output of the signal conditioner feeds a PicoScope 5442A digital sampling oscilloscope [13]. This PC oscilloscope allows easy computer recording of the digitalized strain signals. The DC accuracy of the oscilloscope (in the 20 °C to 30 °C range) with 14 bits mode and $\pm$5 V full scale is

$$u(e_{\text{PS}}(t)) = \pm 1\,\% \text{ of full scale max} \tag{9}$$

which gives the oscilloscope's contribution to the uncertainty on $e(t)$.

The strain gauges are Micro-Measurements EA-06-062AQ-350/E with a gauge length of 0.062 in or 1.57 mm. Small gauges are employed here to minimize the spatial averaging effect due to gauge size. A fuller discussion of the effect of gauge length on cut-off frequencies can be found in [14]. The gauge factor κ is given with 0.5 % uncertainty on its value

$$\frac{u\left(\kappa\right)}{\kappa} = 0.5\,\% \tag{10}$$

The sample is made of 2017 aluminum, carefully machined on a lathe; its length and diameter are known with an accuracy of 0.02 mm (typical caliper graduation)

$$u(l_s) = u(d_s) = 0.02\,\text{mm} \tag{11}$$

The sample length is $l_s = 17.0$ mm and the sample diameter is $d_s = 22.0$ mm.

The distance between the gauge and the specimen/bar interface is 1500 mm for both bars, these distances are accurate to within 0.5 mm.

3 Measurement device uncertainty

The first source of uncertainty arises from the measuring device (see Figure 3). The travelling waves in the SHPB device are measured using strain gauges glued onto the surface of the input and output bars. These strain gauges are handled by a gauge signal conditioner which provides an accurate excitation voltage and amplifies the measured signal. The amplified signal then goes through a digital sampling oscilloscope and is recorded on a computer.

The measurement uncertainties of the strain gauges, gauge conditioner and oscilloscope can be found in their respective technical documentation.

Each bar is equipped with four active strain gauges in full-bridge configuration so that only the axial strain is measured. The strain is computed from the voltage $e(t)$ measured across the bridge

$$\epsilon(t) = \frac{1}{\kappa} \frac{2}{(1+\nu)} \frac{e(t)}{V_{\text{ex}}} \tag{12}$$

where κ is the gauge factor (with a relative uncertainty of 0.5 %) and V_{ex} is the excitation voltage.

The Joint Committee for Guides in Metrology (JCGM) issued a *Guide to the Expression of Uncertainty in Measurement* [15], commonly referred to as GUM, which details the framework for calculating measurement uncertainty. Since the GUM is dense and rather complex, the reader can refer to the didactic introduction by Kirkup and Frenkel [11]. The strain is measured through the functional relationship of Equation (12), and the rules for calculating measurement uncertainty through functional relationship are explained and summarized in [16].

From Equation (12) and reference [16], the measurement uncertainty on the measured strains is therefore

$$\left[\frac{u\left(\epsilon(t)\right)}{\epsilon(t)}\right]^2 = \left[\frac{u\left(\kappa\right)}{\kappa}\right]^2 + \left[\frac{u\left(\nu\right)}{1+\nu}\right]^2 + \left[\frac{u\left(V_{\text{ex}}\right)}{V_{\text{ex}}}\right]^2 + \left[\frac{u\left(e(t)\right)}{e(t)}\right]^2 \tag{13}$$

Actually, the voltage $e(t)$ is not measured directly: it crosses the gauge module and the digital sampling oscilloscope (DSO) before being recorded. The uncertainty on the measured voltage $e(t)$ therefore depends on the measurement uncertainty of the Dewetron gauge module and the measurement uncertainty of the DSO. This writes

$$\left[\frac{u\left(e(t)\right)}{e(t)}\right]^2 = \left[\frac{u\left(e_{\text{HSI}}(t)\right)}{e_{\text{HSI}}(t)}\right]^2 + \left[\frac{u\left(e_{\text{PS}}(t)\right)}{e_{\text{PS}}(t)}\right]^2 \tag{14}$$

as the Dewetron gauge module and the oscilloscope can be viewed as two gain blocks in series (see Figure 3). Equation (14) is numerically evaluated using of Equations (7) and (9).

4 Post treatment uncertainty

The stress and strain in the sample are not directly measured during the test but rather deduced from the waves measured at the middle of the bars. The post-treatment is based on Equations (2) and (3).

The measuring bars have circular cross sections, so Equation (3) is rewritten

$$\sigma_s(t) = \frac{d_b^2 E_b}{d_s^2}\epsilon_t(t) \tag{15}$$

where d_b and d_s are the output bar diameter and sample diameter, respectively. The measurement uncertainty on the stress in the sample $\sigma_s(t)$ is therefore given by

$$\left[\frac{u\left(\sigma_s(t)\right)}{\sigma_s(t)}\right]^2 = 2\left[\frac{u\left(d_b\right)}{d_b}\right]^2 + 2\left[\frac{u\left(d_s\right)}{d_s}\right]^2 + \left[\frac{u\left(E_b\right)}{E_b}\right]^2 + \left[\frac{u\left(\epsilon_t(t)\right)}{\epsilon_t(t)}\right]^2 \tag{16}$$

The measurement uncertainty on the strain in the sample is deduced from Equation (2)

$$\left[\frac{u\left(\epsilon_s(t)\right)}{\epsilon_s(t)}\right]^2 = \left[\frac{u\left(c_0\right)}{c_0}\right]^2 + \left[\frac{u\left(l_s\right)}{l_s}\right]^2 + \left[\frac{u\left(\int_0^t \epsilon_r(\tau)d\tau\right)}{\int_0^t \epsilon_r(\tau)d\tau}\right]^2 \tag{17}$$

Since the signals are sampled and the integration is performed numerically, the integral has to be converted to its discrete time equivalent for numerical post-processing. Replacing continuous time variable t by discrete time variable $n\Delta T$ -where ΔT is the sampling period- in Equation (2) gives

$$\epsilon_s(n\Delta T) = \frac{-2c_0}{l_s}\sum_{i=0}^{n-1}\Delta T\epsilon_r(i\Delta T) \tag{18}$$

Let

$$R_n = \sum_{i=0}^{n-1}\Delta T\epsilon_r(i\Delta T) \tag{19}$$

Assuming that the sampling period ΔT is constant, and since R_n is a sum, the squared standard uncertainty in R_n develops as [16]

$$u^2(R_n) = \Delta T^2\sum_{i=0}^{n-1} u^2\left(\epsilon_r(i\Delta T)\right) \tag{20}$$

Using Equation (19) and Equation (20), Equation (17) is transformed into its discrete form[1]

$$\left[\frac{u\left(\epsilon_s(n\Delta T)\right)}{\epsilon_s(n\Delta T)}\right]^2 = \left[\frac{u\left(c_0\right)}{c_0}\right]^2 + \left[\frac{u\left(l_s\right)}{l_s}\right]^2 + \frac{\sum_{i=0}^{n-1} u^2\left(\epsilon_r(i\Delta T)\right)}{\left(\sum_{i=0}^{n-1}\epsilon_r(i\Delta T)\right)^2} \tag{21}$$

[1] The uncertainty on ϵ_s is computed for the whole curve and only displayed after the time where the stress equilibrium in the sample is achieved.

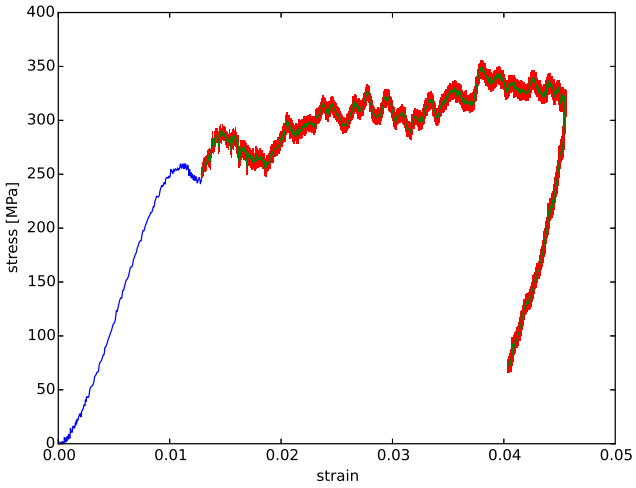

(a)

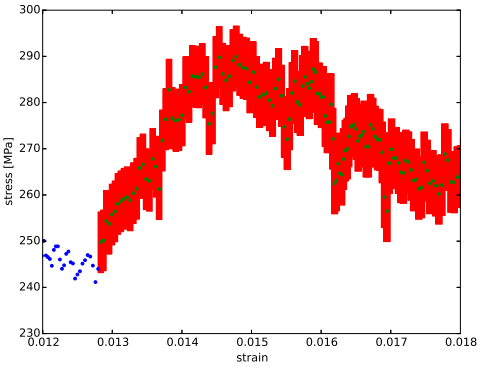

(b)

Fig. 4: Stress strain curve including measurement uncertainties and post-treatment uncertainties: (a) full curve, (b) detail of graphical representation

Note here that the uncertainty on the time step ΔT is very small -the technical documents for the digital sampling oscilloscope[13] give a typical RMS sample jitter of 3 ps- considering the sampling period of 0.2 µs; it is therefore ignored, which greatly simplifies the last term of Equation (21).

Measurement and post-treatment uncertainties are combined in Figure 4, where the uncertainty is shown from the time the sample is at equilibrium. The numerical values employed to produce the graph are given in Section 2.2. A rectangle represents the measurement uncertainty at each sample point,

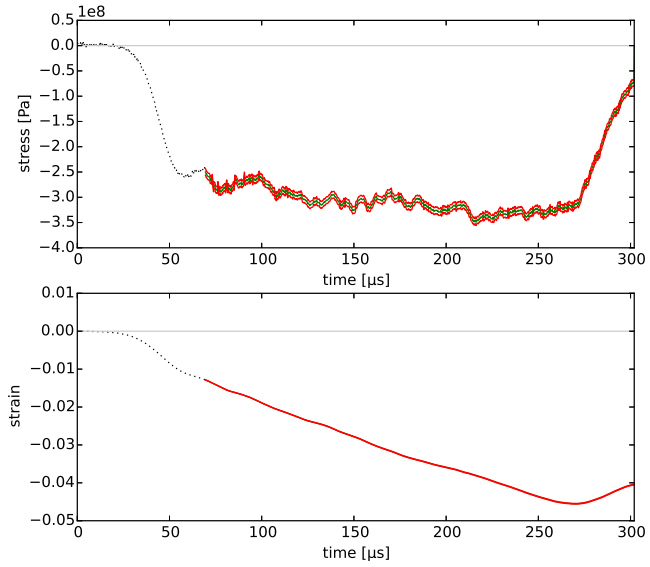

(a)

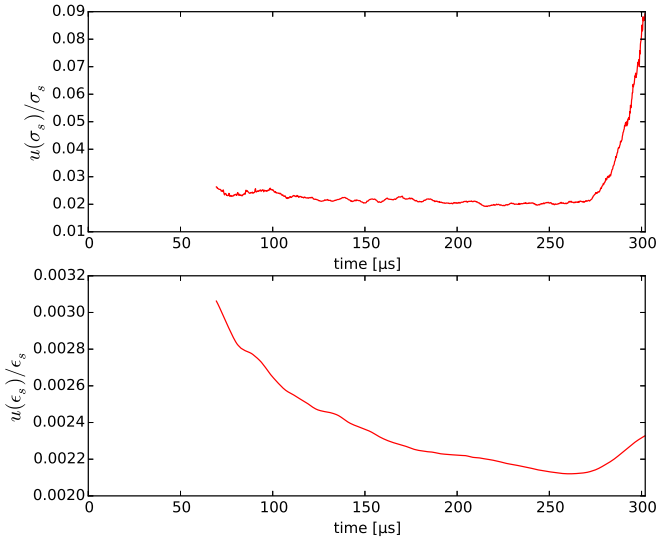

(b)

Fig. 5: (a) Time-history curves of stress and strain in the sample (green curve) with measurement and post-treatment uncertainties (red corridor) starting from time of sample equilibrium. (b) Associated relative uncertainty.

Figure 4b highlights the first points for which the measurement uncertainty is plotted and Figure 5 illustrates the underlying stress and strain time-history signals with the associated measurement and post-treatment uncertainties. Since the sampling rate is very high -5 MS/s, about 1500 points on this specific stress-strain curve- the points are very close and this rectangle method gives a good approximation of the curve envelope.

5 Signal shifting uncertainty

Plotting the stress-strain curve of the sample requires knowledge of the incident, transmitted and reflected waves at the bar-sample interfaces. However, the strain gauges are commonly located in the middle of the measuring bars to avoid superposition of the incident and reflected waves and to ensure uniform stress across the measuring section of the bar. The signals -measured far from the interfaces- are therefore propagated toward the interface with the sample.

The strain signal acquired on the input bar (incident and reflected waves) is measured by a strain gauge located at a distance l_{gi} from the bar-sample interface. According to 1D wave propagation theory, propagating the signal from the gauge to the interface amounts to applying a temporal shift to the signal

$$t_{gi} = \frac{l_{gi}}{c_0} \tag{22}$$

The measurement uncertainty on this shift is therefore

$$\left[\frac{u\left(t_{gi}\right)}{t_{gi}}\right]^2 = \left[\frac{u\left(l_{gi}\right)}{l_{gi}}\right]^2 + \left[\frac{u\left(c_0\right)}{c_0}\right]^2 \tag{23}$$

The same equation holds for the output bar (transmitted signal)

$$\left[\frac{u\left(t_{ig}\right)}{t_{ig}}\right]^2 = \left[\frac{u\left(l_{ig}\right)}{l_{ig}}\right]^2 + \left[\frac{u\left(c_0\right)}{c_0}\right]^2 \tag{24}$$

where l_{ig} is the distance between the strain gauge and the sample face on the output bar.

The strain in the sample $\epsilon_s(t)$ is computed from the reflected wave $\epsilon_r(t)$ in the input bar (see Equation (2)) and the stress in the sample $\sigma_s(t)$ is deduced from the transmitted wave $\epsilon_t(t)$ in the output bar (see Equation (3)). The uncertainty on the position of the stress-strain curve in the stress-strain plane hence combines the temporal uncertainties on propagation in both bars. Given $\Delta t = u(t_{gi}) + u(t_{ig})$, this means that the strain in the sample and the stress in the sample can be moved temporally closer to Δt or farther away from Δt. Figure 6a illustrates the uncertainty on the position of the stress-strain curve induced by the propagation uncertainty. Let $\Delta\sigma_s$ and $\Delta\epsilon_s$ represent the uncertainty on σ_s and ϵ_s due to signal shifting; Figure 6b shows the time series of the relative uncertainties $\Delta\sigma_s/\sigma_s$ and $\Delta\epsilon_s/\epsilon_s$.

The simple approach developed here for propagation uncertainty is based on 1D wave propagation theory. Generally, measured signals are corrected to take into account dispersion effects, which affect the shape of the waves. Bancroft [17] details the velocity of longitudinal waves in cylindrical bars and a summary of dispersion correction is contained in [3]. The forward or backward propagation of the signals requires the use of the Fourier transform to take into account the wavelength dependent-phase velocity [18]. Introducing measurement uncertainty into the dispersion correction would be complicated, whereas this simple 1D non-dispersive wave propagation approach provides a rough estimate of propagation uncertainty.

6 Final stress-strain curve with measurement uncertainties

The equations in Sections 3 and 4 yield the measurement uncertainties on $\epsilon_s(t)$ and $\sigma_s(t)$, assuming there are no additional uncertainties when the measured signals are propagated toward the sample faces. This measurement uncertainty -measurement and post-treatment- is plotted on each of the two extreme curves of Figure 6a, providing an estimate of total measurement uncertainty in Figure 7.

The measurement uncertainty on the stress-strain curve is represented by a single polygonal envelope. This polygonal envelope is the result of the union of all the uncertainty rectangles at each point of the two extreme curves of Figure 6a. The geometric union operation was performed using Angus Johnson's Clipper Library, an efficient open source library for clipping polygons. Each rectangle depicts the uncertainty of the associated point: the width of the rectangle is the strain uncertainty and the height of the rectangle is the stress uncertainty.

The measurement uncertainty is neither constant nor proportional to the signal amplitude because the resulting curve is a parametric plot and because the uncertainty on the measured voltages includes both constant error and proportional error (see Equation (7) for example). Quantifying the measurement uncertainty for the whole curve with a single value is therefore not possible. The uncertainty on the strain is however visually constant on the plateau of the stress-strain curve.

When the strain in the sample reaches 0.04, the stress in the sample is 335 MPa and the envelope of the curve ranges from 319 MPa to 346 MPa. This 13.5 MPa uncertainty is equivalent to $\pm 4.0\,\%$ error on the stress.

Uncertainties on the stress and on the strain are composed of many terms: see for example Equations (16) and (13) for the uncertainty on the stress in the sample. Table 1 lists all contributions to measurement device uncertainty and post-treatment uncertainty $[u(\sigma_s)/\sigma_s]^2$. The highest contribution is from the uncertainty on voltage measurement from the digital sampling oscilloscope (see Equation 9), which could be reduced by using a higher-quality device. However, the signal shifting operation remains another important source of uncertainty: the order of magnitude of the relative uncertainty on the curve

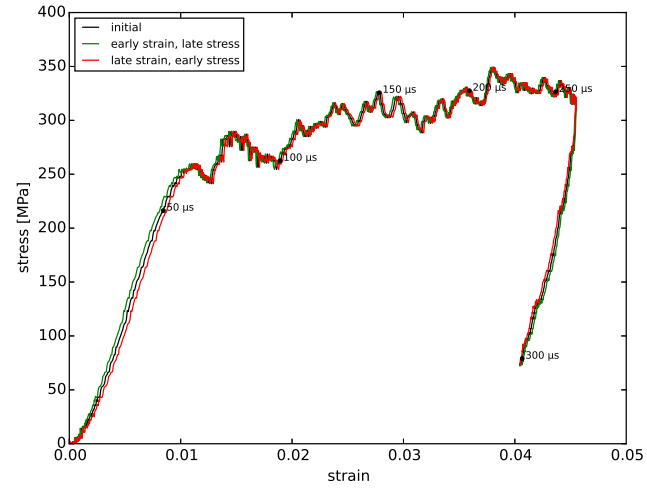

(a)

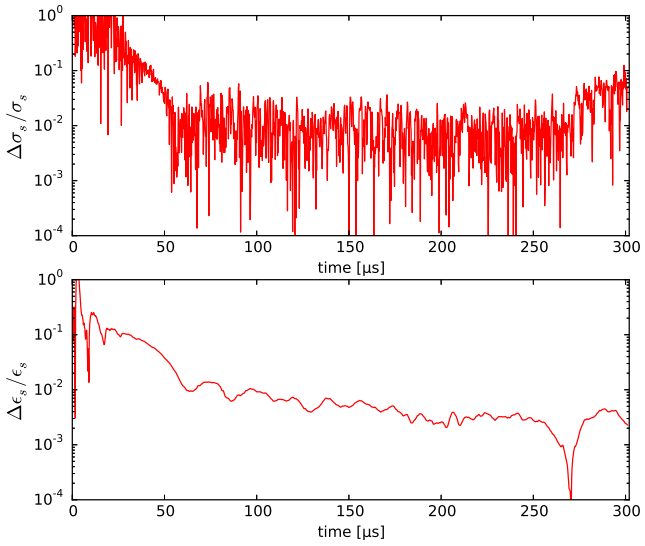

(b)

Fig. 6: Uncertainty on the position of the stress-strain curve caused by uncertainty on the propagation times of the measured signals: (a) full curve, (b) time series of the relative uncertainty due to signal shifting

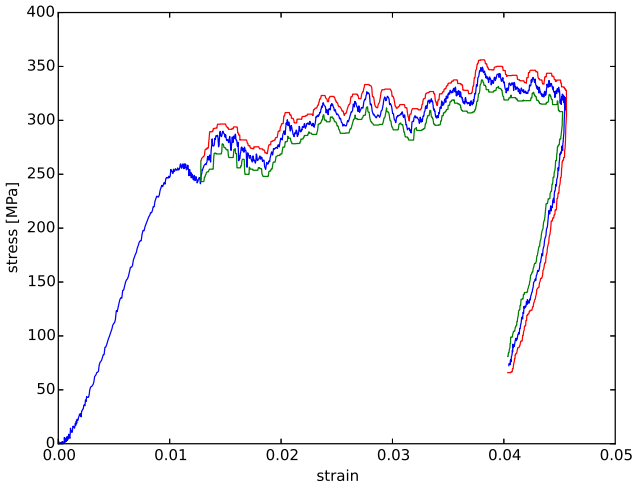

(a)

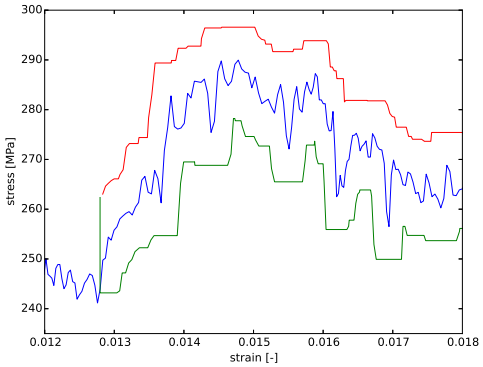

(b)

Fig. 7: Stress-strain curve with measurement, post-treatment and signal shifting uncertainty: (a) full curve, (b) detail

position due to signal shifting alone is 10^{-2} for stress and between 10^{-2} and 10^{-3} for strain (see Figure 6b). And it should be borne in mind that not taking into account the dispersion correction for the measured strains causes signal shifting to be underestimated.

Equation	Calculation	Value
$\left[\frac{u(\sigma_s(t))}{\sigma_s(t)}\right]^2$	-	3.67×10^{-4} (min.)
$= \left[\frac{u(\kappa)}{\kappa}\right]^2$	0.005^2	2.5×10^{-5}
$+ \left[\frac{u(\nu)}{1+\nu}\right]^2$	$(0.0005/1.291)^2$	1.50×10^{-7}
$+ \left[\frac{u(V_{\text{ex}})}{V_{\text{ex}}}\right]^2$	$((0.0003 \times 5 + 0.001)/5)^2$	2.50×10^{-7}
$+ \left[\frac{u(e_{\text{HSI}}(t))}{e_{\text{HSI}}(t)}\right]^2$	see Equation 7	2.89×10^{-6} (min.)
$+ \left[\frac{u(e_{\text{PS}}(t))}{e_{\text{PS}}(t)}\right]^2$	see Equation 9	3.36×10^{-4} (min.)
$+2 \left[\frac{u(d_b)}{d_b}\right]^2$	$2 \times (0.025/31.75)^2$	1.24×10^{-6}
$+2 \left[\frac{u(d_s)}{d_s}\right]^2$	$2 \times (0.02/22)^2$	1.65×10^{-6}
$+ \left[\frac{u(E_b)}{E_b}\right]^2$	$(0.001)^2$	1.0×10^{-6}

Table 1: Decomposition of relative uncertainty on stress: numerical values of the terms of Equations (16) and (13).

7 Conclusion

The measurement uncertainty on stress-strain curves obtained from SHPB tests is, to the authors' knowledge, very rarely assessed. This article introduces a method providing a rough estimate of measurement uncertainty. The uncertainty computed here is most likely underestimated, as this first approximation ignores the uncertainty introduced by the dispersion correction of the measured signals. Results are also based on the assumption that the SHPB setup is employed correctly (no bar or sample misalignment, controlled interface friction, etc. [3]).

The measurement uncertainty estimated by this method is, however, visible on the resulting stress-strain curve: the relative error on the stress in the sample is about 4 %. Such uncertainties can be expected to appear in all experimental work with SHPB, particularly since there is no international standard SHPB setup and each device has its own particular characteristics.

Acknowledgement

The authors would like to thank Stéphane Martinez and Jean-Paul Casano for their technical support.

References

1. H. Kuhn. *ASM Handbook: Volume 8: Mechanical Testing and Evaluation*, volume 8. ASM International, 10 edition, September 2000.
2. R. M. Davies. A Critical Study of the Hopkinson Pressure Bar. *Philosophical Transactions of the Royal Society of London A: Mathematical, Physical and Engineering Sciences*, 240(821):375–457, January 1948.
3. B. A. Gama, S. L. Lopatnikov, and J. W. Gillespie. Hopkinson bar experimental technique: A critical review. *Applied Mechanics Reviews*, 57(4):223, 2004.
4. E.D.H. Davies and S.C. Hunter. The dynamic compression testing of solids by the method of the split Hopkinson pressure bar. *Journal of the Mechanics and Physics of Solids*, 11(3):155–179, May 1963.
5. H. Zhao, G. Gary, and J.R. Klepaczko. On the use of a viscoelastic split hopkinson pressure bar. *International Journal of Impact Engineering*, 19(4):319–330, April 1997. Scopus 60.
6. A. Chawla, S. Mukherjee, R. Marathe, B. Karthikeyan, and R. Malhotra. Determining strain rate dependence of human body soft tissues using a split Hopkinson pressure bar. In *Proceedings of the 2006 International IRCOBI Conference on the Biomechanics of Impact*, 2006.
7. F. Pervin, W. Chen, and T. Weerasooriya. Dynamic compressive response of bovine liver tissues. *Journal of the Mechanical Behavior of Biomedical Materials*, 4(1):76–84, January 2011.
8. Ch. Kranthi Teja, A. Chawla, and S. Mukherjee. Determining the strain rate dependence of cortical and cancellous bones of human tibia using a Split Hopkinson pressure bar. *International Journal of Crashworthiness*, 18(1):11–18, 2013.
9. W. Chen, B. Zhang, and M. J. Forrestal. A split Hopkinson bar technique for low-impedance materials. *Experimental Mechanics*, 39(2):81–85, June 1999.
10. B. Song and W. Chen. Dynamic stress equilibration in split Hopkinson pressure bar tests on soft materials. *Experimental Mechanics*, 44(3):300–312, June 2004.
11. L. Kirkup and B. Frenkel. *An Introduction to uncertainty in measurement: guide to the expression of uncertainty in measurement.* Cambridge Universtity Press, Cambridge, 2006.
12. Dewetron. HSI-STG Isolated universal input module, August 2014.
13. Pico Technology. PicoScope 500 Serie, flexible resolution oscilloscopes, 2013.
14. R. Othman. Cut-off Frequencies Induced by the Length of Strain Gauges Measuring Impact Events. *Strain*, 48(1):16–20, 2012.
15. Evaluation of measurement data – Guide to the expression of uncertainty in measurement. JCGM 100: 2008 (GUM 1995 with minor corrections), BIPM Joint Committee for Guides in Metrology, Paris, Sèvres, 2008.
16. I. Farrance and R. Frenkel. Uncertainty of Measurement: A Review of the Rules for Calculating Uncertainty Components through Functional Relationships. *The Clinical Biochemist Reviews*, 33(2):49–75, May 2012.
17. D. Bancroft. The Velocity of Longitudinal Waves in Cylindrical Bars. *Physical Review*, 59(7):588–593, 1941.
18. J. M. Lifshitz and H. Leber. Data processing in the split Hopkinson pressure bar tests. *International Journal of Impact Engineering*, 15(6):723–733, 1994.